IEEE Access
Multidisciplinary | Rapid Review | Open Access Journal

Received July 21, 2021, accepted August 8, 2021, date of publication August 11, 2021, date of current version August 24, 2021.

Digital Object Identifier 10.1109/ACCESS.2021.3104176

A Duality Based Quasi-Steady-State Model of Three-Phase Five-Limb Sen Transformer

CHAO ZHOU, SONG HAN, (Member, IEEE), NA RONG, AND MIN LIU
Department of Electrical Engineering, Guizhou University, Guiyang 550025, China

Corresponding authors: Song Han (ee.hans@gmail.com) and Na Rong (nrong@gzu.edu.cn)

This work was supported in part by the National Nature Science Foundation of China under Grant 51967004, in part by the program for Top Science and Technology Talents in Universities of Guizhou Province under Grant 2018036, in part by the Guizhou Province Science and Technology Fund under Grant 20191100 and Grant 20210277, and in part by the Guizhou Province Science and Technology Innovation Talent Team Project under Grant 20185615.

ABSTRACT A three-phase five-limb transformer is a potential application form of the Sen Transformer (ST), especially for the scenarios with significantly unbalanced load conditions. This paper proposes a quasi-steady-state model of three-phase five-limb ST (TPFLST) based on duality. Firstly, an equivalent circuit model that takes into account the eddy current effect and the coupling effect involving the magnetic circuit can be derived according to the equivalent magnetic circuit of the TPFLST. The iron-core of the TPFLST may be represented by the parallel combination of the resistances reflecting the power loss of the iron-core and the saturable inductances considering the ferromagnetic hysteresis in virtue of the principle of duality. Subsequently, an electric circuit model of the voltage and current of each winding for the TPFLST is able to be accomplished on the basis of the electrical connection between the TPFLST and the external systems in accordance with Kirchhoff's voltage and current law. Consequently, a quasi-steady-state model of the TPFLST which considers the coupling relationship involving the magnetic and electric circuits can be formed by combining the equivalent circuit model and the electric circuit model. With the help of MATLAB, the effectiveness of the proposed model may be verified by comparing the results about power flow control including power, voltage, and current with the ones from the existing literature. Furthermore, the TPFLST is found to be better-suited for the unbalanced load condition according to a comparison among the unbalanced degrees of output currents for the STs with different core structures under unbalanced load conditions.

INDEX TERMS Principle of duality, three-phase five-limb, Sen Transformer, quasi-steady-state model, unbalanced load, series-compensating voltage.

I. INTRODUCTION

Recently, the demand for electricity of the power system makes the transition into renewable energy sources an inevitable choice due to the rising prices of energy, fossil fuel depletion, and the increasing concerns about the environment [1]–[3]. Owing to the volatility, intermittency, and uncertainty of renewable energy, they bring great challenges to the security and stability of the power network [4]–[6]. Therefore, in order to ensure safe, stable, and cost-effective power supply, it is an urgent need for a flexible power flow control device to enhance the transmission ability of the existing power network [7].

The unified power flow controller (UPFC) is one of the most representative and comprehensive devices in flexible AC transmission systems (FACTS), but the high installation and operation costs might hamper its widespread applications. Compared with the converter based UPFC, "Sen" Transformer (ST) proposed by K. K. Sen originates from phase-shifting transformer, which is almost capable of providing the same independent active and reactive power flow control as the UPFC [8]. The advantages of ST include low cost, large capacity, and high reliability [9]–[11]. Whereas it is hardly to achieve accurate power flow control. As a consequence, some novel topologies of the ST were proposed in [7], [12]–[15], which combine the advantages of large capacity and high reliability of the ST, and the flexible adjustment of UPFC for improving the ability of power flow control, such as the improved hybrid unified power flow controller (IHUPFC), the power transistor-assisted "Sen" transformer (TAST), and the hybrid electromagnetic unified power flow controller (HEUPFC). Besides, a new variant of

The associate editor coordinating the review of this manuscript and approving it for publication was Poki Chen.

This work is licensed under a Creative Commons Attribution 4.0 License. For more information, see https://creativecommons.org/licenses/by/4.0/

ST with the reverse-phase adjustment of tap changer was proposed, which may improve the control range and the accuracy of voltage regulation by increasing the number of operating points for the tap-changers of secondary windings [16], [17].

From the perspective of the modeling method for transformer, there are mainly two types of methods, i.e., the principle of duality-based method and the unified magnetic equivalent circuit (UMEC) based method. Both modeling approaches are based on the magnetic equivalent circuit theory [18]. The principle of duality was first introduced by Cherry [19], which has been widely applied to transformer modeling. The equivalent circuit models of the three-phase three-limb and the three-phase five-limb were built in [20] and [21] on the basis of duality. A detailed transformer model using duality was established in [22], which considered the topological structures of iron-core, air gap, and tank. The most common method of the duality-based model and its application for a transformer with a special winding structure were discussed in [23]. Nevertheless, there is no comprehensive research on ST modeling in virtue of the principle of duality. From the perspective of the iron-core structure for ST, previous studies were mainly focused on single-phase transformer bank or three-phase three-limb structure. For the sake of developing those models and methods suitable for power system steady analysis, a steady-state model of the EST for unified iterative power flow solution was established in [24]. A kind of control strategy for the tap-changers was proposed in [25], which can fulfill an optimal combination of tap-settings for the voltage compensating windings of the ST. For the purpose of understanding the transient behavior in the commutation process for the EST, a switching transient model of the EST was built in [26]. The models of the ST and its variants mentioned above are composed of nine single-phase transformers. Moreover, an analytical electromagnetic model considering the multi-winding magnetic coupling for the ST was presented in [27] so as to analyze the internal characteristics of the ST. In order to analyze the internal and external characteristics of ST, a detailed real-time electromagnetic transient model of the ST was proposed in [28]. Meanwhile, its real-time simulation was implemented by the C programming in MATLAB/SIMULINK environment. An electromagnetic transient (EMT) model of ST utilizing real-time high-fidelity nonlinear magnetic equivalent circuit (MEC) was proposed in [29]. Its real-time simulation was demonstrated on the field-programmable gate array (FPGA). Besides, the quasi-steady-state models of UPFC and static synchronous compensator (STATCOM) were established in [30] and [31] respectively for analyzing voltage collapse and transient stability. Nevertheless, there are rarely reports about the quasi-steady-state model of the ST. In the literature mentioned above, the iron-cores of the STs also belong to the three-phase three-limb structure. However, the three-phase five-limb transformer is usually adopted for the specific large-capacity requirements considering the limitations in the aspects of transportation and installation [32]. In addition, there are sometimes quite a few electromagnetic loops in the high-voltage distribution systems due to the characteristics of meshed structure such as some 220kV/110kV urban distribution systems in China [33]. Therefore, the three-phase five-limb Sen Transformer (TPFLST) is probably a potential application form, which should be investigated.

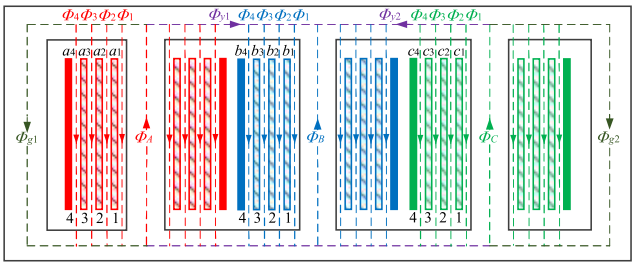

FIGURE 1. An Iron-core structure of the TPFLST.

The objective of this paper is to propose a quasi-steady-state model of the TPFLST. In accordance with the principle of duality, the equivalent circuit model of TPFLST may be a complex combination of ideal transformers, resistances, and inductances. The contributions of this paper are (1) A quasi-steady-state model of the ST with three-phase five-limb iron-core structure is proposed. (2) The model is built on the basis of the principle of duality, which takes into account the eddy current effect and the coupling effect involving the magnetic circuit. (3) The differences involving the unbalanced degrees of output currents between the three-phase three-limb ST (TPTLST) and the TPFLST under unbalanced load conditions are presented.

This paper is organized as follows. Section 2 describes what is the quasi-steady-state model of the TPFLST and how to determine the associated parameters. In Section 3, Case 1(a) shows the four-quadrant adjustment of power flow, and Case 1(b) illustrates the adjustment of series-compensating voltage from the proposed model and compares them with the results of simulation experiments from [25]. Case 2 presents the comparisons about unbalanced degrees of output currents among the STs with different iron-core structures. The conclusions are drawn in Section 4.

II. A QUASI-STEADY-STATE MODEL FOR THE TPFLST

A. AN EQUIVALENT MAGNETIC CIRCUIT FOR THE TPFLST

The winding arrangement and the magnetic flux distribution of the TPFLST are illustrated in Fig. 1, which is inspired by the three-phase five-limb transformer in [34]. The solid rectangles represent the primary windings of phases A, B, and C (a_4, b_4, and c_4), the skew lines rectangles represent the secondary windings of phases A, B, and C (a_1 to a_3, b_1 to b_3, and c_1 to c_3). Φ_A, Φ_B, and Φ_C denote the main magnetic flux of the ST, respectively. Φ_{y1} and Φ_{y2} denote the magnetic flux of yoke between phase A and phase B, and phase B and phase C, respectively. Φ_{g1} and Φ_{g2} denote the magnetic flux of end limbs and end yokes, respectively. Φ_1 stands for the leakage flux between the first windings (a_1, b_1, and c_1) and the limbs (A, B, and C). Φ_2 stands for the leakage flux between the first windings (a_1, b_1, and c_1) and the second windings (a_2,

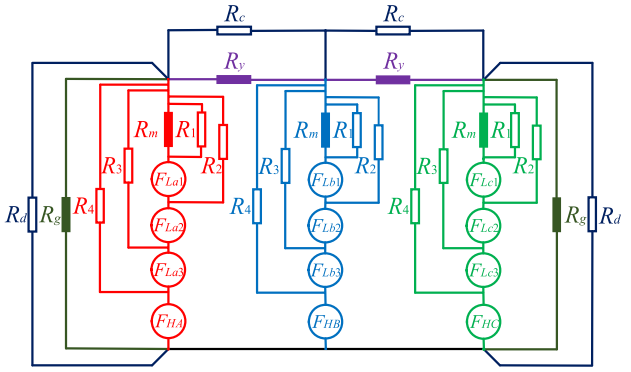

FIGURE 2. An equivalent magnetic circuit of the TPFLST.

b_2, and c_2). Φ_3 indicates the leakage flux between the second windings (a_2, b_2, and c_2) and the third windings (a_3, b_3, and c_3). Φ_4 indicates the leakage flux between the third windings (a_3, b_3, and c_3) and the fourth windings (a_4, b_4, and c_4).

On the basis of the magnetic flux distribution, an equivalent magnetic circuit of the TPFLST is revealed in Fig. 2. F_{HA}, F_{HB}, and F_{HC} denote the magnetomotive force of the primary windings in phase A, B, and C, separately. F_{La1} to F_{La3}, F_{Lb1} to F_{Lb3}, and F_{Lc1} to F_{Lc3} denote the magnetomotive force of the secondary windings in phase A, B, and C, separately. The solid rectangles mean the reluctances with flux paths through the iron: R_m for the limbs, R_y for the yokes, R_g for the end limbs and their yokes. The open rectangles mean the reluctances with flux paths in the air. R_1 for the paths between the limbs (A, B, and C) and the first windings (a_1, b_1, and c_1), R_2 for the paths between the first windings (a_1, b_1, and c_1) and the second windings (a_2, b_2, and c_2), R_3 for the paths between the second windings (a_2, b_2, and c_2) and the third windings (a_3, b_3, and c_3), R_4 for the paths between the limbs and the space between the third windings (a_3, b_3, and c_3) and the fourth windings (a_4, b_4, and c_4), R_c for the leakage path through the air in parallel with the yokes, R_d for the leakage path through the air in parallel with the end limbs.

B. THE DUALITY BASED EQUIVALENT CIRCUIT MODEL FOR THE TPFLST

The reluctances with the flux paths through iron-core are able to be transformed into a set of nonlinear inductances by the principle of duality [19]. On the contrary, the reluctances with the flux paths in air can be transformed into a group of linear inductances [20], [21]. Fig. 3 manifests an equivalent circuit model of the TPFLST that may reflect the relationship between the electric circuit and the magnetic circuit.

As for the equivalent circuit model in Fig. 3, R_A, R_B, and R_C denote the winding resistances of the primary windings in phase A, B, and C, separately. R_{La1} to R_{La3}, R_{Lb1} to R_{Lb3}, and R_{Lc1} to R_{Lc3} denote the winding resistances of the secondary windings in phase A, B, and C, separately. The linear inductances L_{f12}, L_{f23}, and L_{f34} ($f = a, b, c$) represent the flux leakages between both windings. The linear inductances L_{a1}, L_{b1}, L_{c1}, L_d, and L_c represent the flux leakages in parallel with iron-core. In this way, the iron-core for the TPFLST

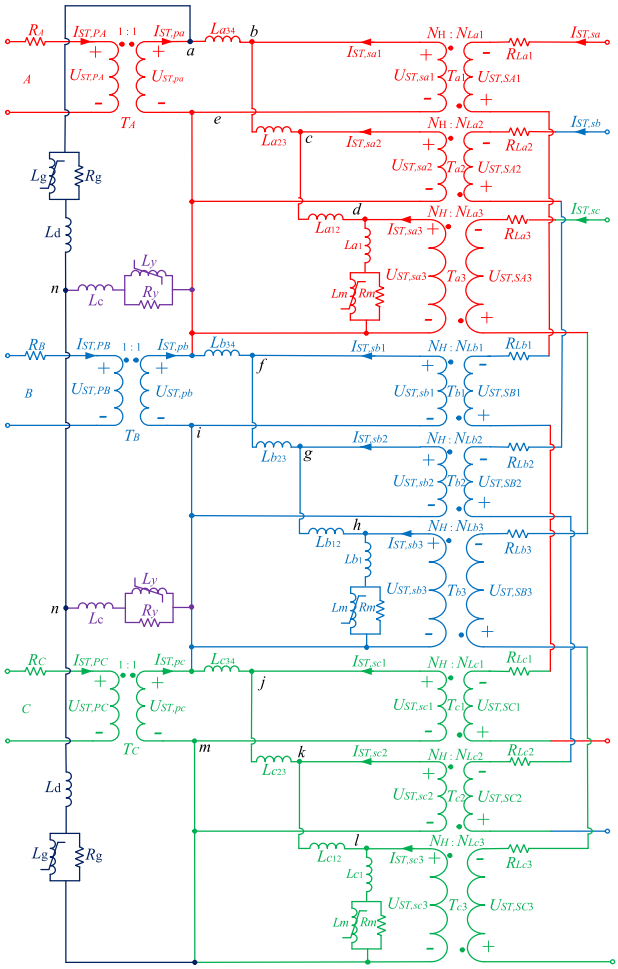

FIGURE 3. A Duality based equivalent circuit for the TPFLST.

could be represented through the parallel combination of the resistance R_m which reflects the loss of iron-core and the saturable inductance L_m which considering the ferromagnetic hysteresis. Similarly, the parallel combination of R_y and L_y indicates the yoke section between a pair of phases. The parallel combination of R_g and L_g indicates the section of end limbs and their yokes. N_H indicates the turns of the primary windings in phase A, B, and C. N_{La1} to N_{La3}, N_{Lb1} to N_{Lb3}, and N_{Lc1} to N_{Lc3} mean the turns of the secondary windings in phase A, B, and C, separately. T_A, T_B, and T_C mean the ideal single-phase transformer on the primary side, separately. T_{a1} to T_{a3}, T_{b1} to T_{b3} and T_{c1} to T_{c3} mean the ideal single-phase transformer on the secondary side, separately.

According to the equivalent circuit model in Fig. 3, the nodal voltage equation is defined by (1).

$$\begin{bmatrix} I_{ST,s1} \\ I_{ST,s2} \\ \vdots \\ I_{ST,s13} \end{bmatrix} = \begin{bmatrix} y_{1,1} & y_{1,2} & \cdots & y_{1,13} \\ y_{2,2} & y_{2,2} & \cdots & y_{2,13} \\ \vdots & \vdots & & \vdots \\ y_{13,1} & y_{13,2} & \cdots & y_{13,13} \end{bmatrix} \begin{bmatrix} U_a \\ U_b \\ \vdots \\ U_m \end{bmatrix} \quad (1)$$

where the injection currents of nodes are represented by from $I_{ST,s1}$ to $I_{ST,s13}$, the admittances of branches are represented

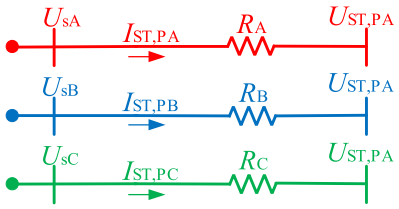

FIGURE 4. A three-phase equivalent circuit for the primary windings of the TPFLST.

by from $y_{1,1}$ to $y_{13,13}$, and the voltages to ground of nodes are represented by from U_a to U_m, respectively.

The voltage and current equations for three ideal transformers (T_A, T_B, and T_C) on the primary side in Fig. 3 can be acquired by (2).

$$\begin{cases} \boldsymbol{I_{ST,P}} = \boldsymbol{I_{ST,p}} \\ \boldsymbol{U_{ST,P}} = \boldsymbol{U_{ST,p}} \end{cases} \tag{2}$$

where $\boldsymbol{I_{ST,P}}$ and $\boldsymbol{I_{ST,p}}$ denote the current matrix at the primary side and the current matrix at the secondary side for the three ideal transformers, separately. Meanwhile, $\boldsymbol{U_{ST,P}}$ and $\boldsymbol{U_{ST,p}}$ denote the voltage matrix at the primary side and the voltage matrix at the secondary side for the three ideal transformers, separately. Furthermore, the four variables may be described as below.

$$\boldsymbol{I_{ST,P}} = [I_{ST,PA}(t), I_{ST,PB}(t), I_{ST,PC}(t)]^{\mathrm{T}} \tag{3}$$
$$\boldsymbol{I_{ST,p}} = [I_{ST,pa}(t), I_{ST,pb}(t), I_{ST,pc}(t)]^{\mathrm{T}} \tag{4}$$
$$\boldsymbol{U_{ST,P}} = [U_{ST,PA}(t), U_{ST,PB}(t), U_{ST,PC}(t)]^{\mathrm{T}} \tag{5}$$
$$\boldsymbol{U_{ST,p}} = [U_{ST,pa}(t), U_{ST,pb}(t), U_{ST,pc}(t)]^{\mathrm{T}} \tag{6}$$

The voltage and current equations of nine ideal transformers (T_{a1} to T_{a3}, T_{b1} to T_{b3}, and T_{c1} to T_{c3}) at the secondary side in Fig.4 can be expressed as (7).

$$\begin{cases} \boldsymbol{I_{ST,S}} = -\boldsymbol{K}^{-1}\boldsymbol{I_{ST,s}} \\ \boldsymbol{U_{ST,S}} = \boldsymbol{K}\boldsymbol{U_{ST,s}} \end{cases} \tag{7}$$

where $\boldsymbol{K}$ is a diagonal 9×9 matrix. $\boldsymbol{I_{ST,S}}$ and $\boldsymbol{I_{ST,s}}$ stand for the primary-side current matrix and the secondary-side current matrix about the nine ideal transformers, respectively. $\boldsymbol{U_{ST,S}}$ and $\boldsymbol{U_{ST,s}}$ stand for the primary-side voltage matrix and the secondary-side voltage matrix about the nine ideal transformers, respectively. So $\boldsymbol{I_{ST,S}}$, $\boldsymbol{I_{ST,s}}$, $\boldsymbol{U_{ST,S}}$, $\boldsymbol{U_{ST,s}}$ and $\boldsymbol{K}$ are defined as followings.

$$\boldsymbol{K} = diag[k_1, k_2, k_3, k_4, k_5, k_6, k_7, k_8, k_9] \tag{8}$$
$$\boldsymbol{I_{ST,S}} = [I_{ST,sa}(t), I_{ST,sa}(t), I_{ST,sa}(t), I_{ST,sb}(t), I_{ST,sb}(t), I_{ST,sb}(t), I_{ST,sc}(t), I_{ST,sc}(t), I_{ST,sc}(t)]^{\mathrm{T}} \tag{9}$$
$$\boldsymbol{I_{ST,s}} = [I_{ST,sa1}(t), I_{ST,sb1}(t), I_{ST,sc1}(t), I_{ST,sa2}(t), I_{ST,sb2}(t), I_{ST,sc2}(t), I_{ST,sa3}(t), I_{ST,sb3}(t), I_{ST,sc3}(t)]^{\mathrm{T}} \tag{10}$$
$$\boldsymbol{U_{ST,S}} = [U_{ST,SA1}(t), U_{ST,SB1}(t), U_{ST,SC1}(t), U_{ST,SA2}(t), U_{ST,SB2}(t), U_{ST,SC2}(t), U_{ST,SA3}(t), U_{ST,SB3}(t), U_{ST,SC3}(t)]^{\mathrm{T}} \tag{11}$$
$$\boldsymbol{U_{ST,s}} = [U_{ST,sa1}(t), U_{ST,sb1}(t), U_{ST,sc1}(t), U_{ST,sa2}(t), U_{ST,sb2}(t), U_{ST,sc2}(t), U_{ST,sa3}(t), U_{ST,sb3}(t), U_{ST,sc3}(t)]^{\mathrm{T}} \tag{12}$$

The voltage supplementary equations for twelve ideal transformers in Fig. 3 should be obtained by (13).

$$\begin{cases} U_a - U_e = U_{ST,pa} \\ U_e - U_i = U_{ST,pb} \\ U_i - U_m = U_{ST,pc} \end{cases} \text{(a)} \quad \begin{cases} U_b - U_e = U_{ST,sa1} \\ U_c - U_e = U_{ST,sa2} \\ U_d - U_e = U_{ST,sa3} \end{cases} \text{(b)}$$
$$\begin{cases} U_f - U_i = U_{ST,sb1} \\ U_g - U_i = U_{ST,sb2} \\ U_h - U_i = U_{ST,sb3} \end{cases} \text{(c)} \quad \begin{cases} U_j - U_m = U_{ST,sc1} \\ U_k - U_m = U_{ST,sc2} \\ U_l - U_m = U_{ST,sc3} \end{cases} \text{(d)} \tag{13}$$

C. THE ELECTRIC CIRCUIT MODEL FOR THE TPFLST INTEGRATED INTO TRANSMISSION NETWORK

The relationship of the electrical connection between the TPFLST and the transmission network is exhibited in Fig. 12 in the Appendix. In accordance with the electrical connection between them, equations (14) and (15) are derived by using Kirchhoff's voltage and current law.

$$\begin{cases} I_{ST,a} = I_{ST,sa} + I_{ST,PA} \\ I_{ST,b} = I_{ST,sb} + I_{ST,PB} \\ I_{ST,c} = I_{ST,sc} + I_{ST,PC} \end{cases} \tag{14}$$
$$\begin{cases} U_{sa} = I_{ST,a}Z_s + U_{sA} \\ U_{sb} = I_{ST,b}Z_s + U_{sB} \\ U_{sc} = I_{ST,c}Z_s + U_{sC} \end{cases} \tag{15}$$

where $I_{ST,a}$, $I_{ST,b}$, and $I_{ST,c}$ represent the currents from the sending-end in phase A, B, and C, separately. $I_{ST,PA}$, $I_{ST,PB}$, and $I_{ST,PC}$ represent the current of primary windings in phases A, B, and C, separately. $I_{ST,sa}$, $I_{ST,sb}$, and $I_{ST,sc}$ are the current of secondary windings in phases A, B, and C, separately. U_{sa}, U_{sb}, and U_{sc} are the sending-end voltage in phase A, B, and C, separately. U_{sA}, U_{sB}, and U_{sC} denote the terminal voltages of the primary windings in phases A, B, and C, separately. Z_s denotes the sending-end impedance.

Fig. 4 exhibits the three-phase equivalent electric circuit for the primary winding of the TPFLST. On the basis of the equivalent circuit model in Fig. 4, the following equation is able to be attained.

$$\begin{cases} U_{sA} = I_{ST,PA}R_A + U_{ST,PA} \\ U_{sB} = I_{ST,PB}R_B + U_{ST,PB} \\ U_{sC} = I_{ST,PC}R_C + U_{ST,PC} \end{cases} \tag{16}$$

where $U_{ST,PA}$, $U_{ST,PB}$, and $U_{ST,PC}$ represent the terminal voltages of three ideal transformers at the primary side in phases A, B, and C, respectively.

The three-phase equivalent electric circuit for the secondary windings of the ST is demonstrated in Fig. 5. In the light of the series connection in the transmission network

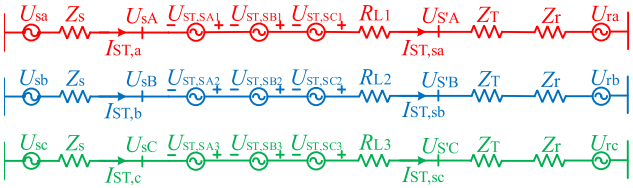

FIGURE 5. A three-phase equivalent circuit for the secondary windings of the TPFLST.

from the sending-end to the receiving-end, equation (17) is established.

$$\begin{cases} U_{sa} - I_{ST,a}Z_s + U_{ST,SA1} + U_{ST,SB1} + U_{ST,SC1} \\ -I_{ST,sa}(R_{L1} + Z_T + Z_r) - U_{ra} = 0 \\ U_{sb} - I_{ST,b}Z_s + U_{ST,SA2} + U_{ST,SB2} + U_{ST,SC2} \\ -I_{ST,sb}(R_{L2} + Z_T + Z_r) - U_{rb} = 0 \\ U_{sc} - I_{ST,c}Z_s + U_{ST,SA3} + U_{ST,SB3} + U_{ST,SC3} \\ -I_{ST,sc}(R_{L3} + Z_T + Z_r) - U_{rc} = 0 \end{cases} \tag{17}$$

where $U_{ST,SA1}$, $U_{ST,SB1}$, $U_{ST,SC1}$, $U_{ST,SA2}$, $U_{ST,SB2}$, $U_{ST,SC2}$, $U_{ST,SA3}$, $U_{ST,SB3}$, and $U_{ST,SC3}$ represent the terminal voltages of nine ideal transformers at the secondary side in phases A, B, and C, respectively. U_{ra}, U_{rb}, and U_{rc} represent the receiving-end voltage in phases A, B, and C, respectively. Z_T stands for the impedance of the transmission line. Z_r stands for the receiving-end impedance. R_{L1}, R_{L2}, and R_{L3} stand for the equivalent resistances of the second windings in phases A, B, and C, respectively.

$$\begin{cases} R_{L1} = R_{La1} + R_{Lb1} + R_{Lc1} \\ R_{L2} = R_{La2} + R_{Lb2} + R_{Lc2} \\ R_{L3} = R_{La3} + R_{Lb3} + R_{Lc3} \end{cases} \tag{18}$$

In this way, the quasi-steady-state model for the TPFLST is able to be solved by combining (1) – (18). Subsequently, all the voltages and currents of the primary and secondary windings would be deduced.

D. PARAMETERS DETERMINATION

The parameters of the equivalent circuit model in Fig. 3 could be obtained from the testing measurements, which include the leakage reactance between two windings and the resistance that represents the loss of the iron-core. Certainly, they can be also estimated from the design parameters of the TPFLST if there is no prototype.

1) CORE PARAMETERS

The silicon steel sheet generates an eddy current in the alternating magnetic field. Thus, the property of the core should be described by complex permeability [35] when the eddy current effect is taken into account. The nonlinear reluctances R in Fig. 3 is represented by the parallel combination of equivalent nonlinear inductance L_{eq} and resistance R_{eq} after using the principle of duality, given as [36].

$$\begin{cases} L_{eq} = \mathrm{Re}(N^2\mu_r\mu_0 wd\tanh(p)/(ps)) \\ R_{eq} = \mathrm{Im}(N^2\mu_r\mu_0 wd\tanh(p)/(ps)) \end{cases} \tag{19}$$

TABLE 1. Data for the electrical system.

Parameter	Value
Base value	138 kV
Rating capacity	160MVA
Sending-end line-to-line voltage	$1\angle 0^o$ p.u.
Receiving-end line-to-line voltage	$1\angle$-20° p.u.
Source impedance at the sending-end	1.0053 Ω,19.17 mH
Source impedance at the receiving-end	0 Ω,0 mH
Transmission line impedance	3.0159 Ω,59.19 mH
Frequency	60 Hz

where d, s, and w stand for the thickness, length, and width of the silicon steel lamination, separately. μ_r stands for relative permeability. μ_0 is permeability of free space, and N is the turns of winding. Moreover,

$$p = \frac{\gamma d}{2} \tag{20}$$

$$\gamma = \sqrt{j\omega\mu_r\mu_0\sigma} \tag{21}$$

where σ represents conductivity.

2) LEAKAGE INDUCTANCE PARAMETERS

The leakage inductances between two windings can be obtained from the design parameters [32].

$$\begin{cases} L_{s12} = \dfrac{\mu_0\pi N_1^2}{l_c}\left(\dfrac{D_1d_1}{3} + D_{12}d_{12} + \dfrac{D_2d_2}{3}\right) \\ L_{s23} = \dfrac{\mu_0\pi N_2^2}{l_c}\left(\dfrac{D_2d_2}{3} + D_{23}d_{23} + \dfrac{D_3d_3}{3}\right) \\ L_{s34} = \dfrac{\mu_0\pi N_3^2}{l_c}\left(\dfrac{D_3d_3}{3} + D_{34}d_{34} + \dfrac{D_4d_4}{3}\right) \end{cases} \tag{22}$$

where L_{s12}, L_{s23}, and L_{s34} represent the leakage inductances of the space between two windings, separately. N_1, N_2, and N_3 represent the turns of winding a_1, a_2, and a_3, separately. l_c represents the mean length of the magnetic flux path. d_1, d_2, d_3, and d_4 are the width of windings, separately. d_{12}, d_{23}, and d_{34} are the width between two windings, separately. D_1, D_2, D_3, and D_4 are the mean diameters of windings, separately. D_{12}, D_{23}, and D_{34} are the mean diameters of the space between two windings, separately.

III. CASE STUDIES

A. CASE 1: THE REGULATION OF POWER FLOW AND SERIES-COMPENSATING VOLTAGE

For the sake of verifying the effectiveness of the proposed model, there are some analytical calculations about the series-compensating voltage and power flow for a three-phase five-limb transformer. Generally, the thickness and the relative permeability of the silicon steel sheet range from 0.23mm to 0.35mm and from 7000 to 10000, respectively. The thickness and the relative permeability of the silicon steel sheet are 0.3mm and 10000 in this paper [37], [27]. The parameters of the electrical system and the TPFLST are listed in Table 1 and Table 2.

TABLE 2. Data for the physical structure of the TPFLST.

Parameter	Value
Length of the leg	7.18 m
Cross-sectional area of iron-core	0.454 m^2
Length of the yoke	2.66 m
Cross-sectional area of yoke	0.454 m^2
Length of the end yoke	1.33 m
Length of the end limb	7.18 m
Leakage inductance $L_{f12}/L_{f23}/L_{f34}$	1.1019/0.8629/0.6785 mH
Leakage inductance L_{a1}, L_{b1}, $L_{c1}/L_d/L_c$	3.136/32.2/95.26 mH
Saturable inductance $L_m/L_y/L_g$	81.92/40.96/122.88 H
Resistance $R_m/R_y/R_g$	245.76/122.88/368.64 kΩ
Resistance and inductance of the ST	1.7854 Ω,47.4 mH
Turns of primary winding of the ST	64
Turns of second winding of the ST	26
Number of taps for ST	4
Maximum position of tap for the ST	0.4 p.u.
Adjustment time of tap for the ST	1 s/step

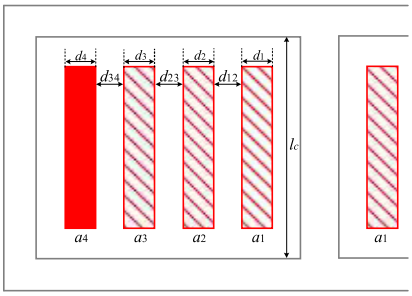

FIGURE 6. The geometrical arrangement of windings in the TPFLST window.

1) THE ADJUSTMENT OF POWER FLOW

Calculation of the series-compensating voltage of 0.1 p.u. to 0.4 p.u. was performed at different β. The phase angle β was varied at a discrete step of 60° in the range of 0° to 360°. The variation of both the active power P_r and the reactive power Q_r at the receiving end is revealed in Fig. 7.

It is obviously seen from Fig. 7 that there are six points at $\beta = 0°$, 60°, 120°, 180°, 240°, and 300°, only at these points, the injected series-compensating voltage is close to the required series-compensating voltage. The series-compensating voltage is supplied by only one winding when the angle β at 0°, 120°, and 240°, while the angle β at 60°, 180°, and 300°, the series-compensating voltage is supplied by two windings. For example, if the injected series-compensating voltage in phase a is 0.2 p.u. and angle is 60°, the voltage would be supplied by both phase a and phase c, each voltage is 0.2 p.u.. In addition, the active power P_r and reactive power Q_r for the proposed model can achieve the four-quadrant adjustment, which verifies the effectiveness for the proposed model. However, during the injected series-compensating voltage, the load in the transmission line may be changed. Besides, the Thevenin equivalent impedance at the compensation point and the parallel load at the exciter unit of the ST might be varied with the changing of tap-positions. They would cause the difference between the $P_r - Q_r$ curves in Fig. 7 and the regular hexagon.

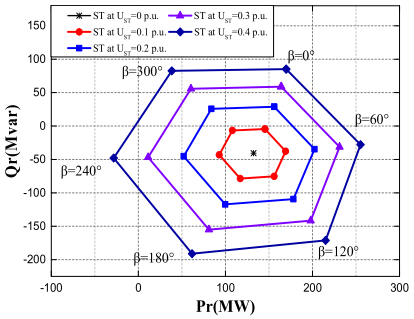

FIGURE 7. Relationship between Pr and Qr at various phase angle and series voltage U_{ST} for the TPFLST.

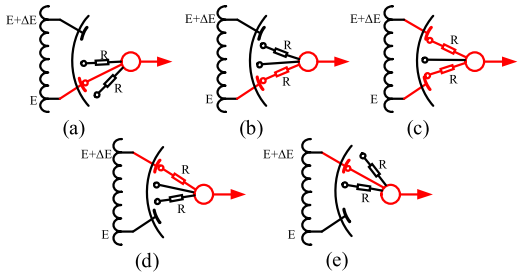

FIGURE 8. Switching sequence from tap position 2 (0.2 p.u.) to tap position 3 (0.3 p.u.) in an OLTC with a diverter switch and selector.

2) THE ADJUSTMENT OF SERIES-COMPENSATING VOLTAGE

Performing series-compensating voltage according to the voltage regulation method in [25], for instance, when $t < 5$ s, $U_{ST,A} = 0$ p.u., $\beta = 0°$; when 5 s $< t <$ 14 s, $U_{ST,A} =$ 0.2 p.u., $\beta = 120°$; when 14 s $< t <$ 23 s, $U_{ST,A} = 0.2$ p.u., $\beta = 60°$; when 23 s $< t <$ 32 s, $U_{ST,A} = 0.4$ p.u., $\beta = 60°$. The type of On-load Tap Changer (OLTC) is a dual-resistance structure. The time required to move the tap selector between adjacent tap positions is 1 s, there are four steps of approximately 0.25 s each are performed, the transition resistance is 10 Ω [38]. The switching process is illustrated in Fig. 8 [39].

The series-compensating voltage $U_{ST,A}$ of the TPFLST is demonstrated in Fig. 9a. The secondary winding current $I_{ST,sa}$ of the TPFLST is displayed in Fig. 9b. In addition, the series-compensating voltage $U_{s'sa}$ and the secondary winding current $I_{s'sa}$ in [25] are also manifested in Fig. 9 for comparison.

Fig. 9 manifested that the trends of $U_{ST,A}$ and $I_{ST,sa}$ are similar to the results in [25], the series-compensating voltage $U_{ST,A}$ and the secondary winding current $I_{ST,sa}$ are able to reach the expected values. The maximum error of the series-compensating voltage does not exceed 2.03%, and the maximum error of secondary winding current does not exceed 2.9%. The errors are within the allowable range, which further verifies the effectiveness for the proposed model. However, there are some differences in the comparison result. On the one hand, when the transition resistor is connected to the circuit, the current through the secondary winding will start to decrease. When the tap changer operates to step (c) in Fig.8, two transition resistors are connected in parallel, which results in a slower decrease for the current. When the transition resistor is removed, the current in the secondary winding

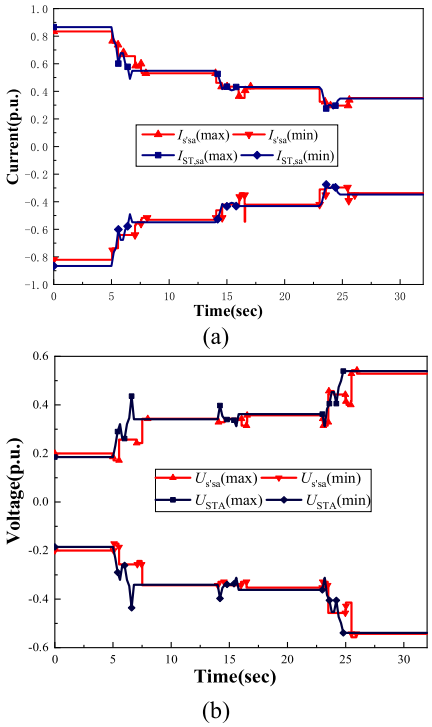

FIGURE 9. Injected series-compensating voltages and secondary winding currents of the TPFLST during the tap-changing process (a) Variation of the injected voltage on phase A of the TPFLST. (b) Variation of the secondary winding currents on phase A of the TPFLST.

will rise. The trend of the series-compensating voltage is opposite to the trend of the current. On the other hand, the quasi-steady-state model of the TPFLST in this paper, which takes into account not only the phase-to-phase magnetic coupling but also the eddy current effect. The iron-core of the ST in [25] is the nine-single-phase transformer bank structure and the three-phase magnetic circuit is independent of each other. It should be noticed that the saturation and hysteresis characteristics of the iron-core are neglected so as to simplify the calculations.

B. CASE 2: COMPARISONS AMONG THE STS WITH DIFFERENT CORE STRUCTURES UNDER UNBALANCED LOAD CONDITIONS

In order to evaluate the performance of the TPTLST and the TPFLST with unbalanced load conditions, the unbalanced degrees of output currents for the TPTLST and the TPFLST with different compensation states should be compared. Eventually, the comparing results prove that the TPFLST can be applied to the scenario with an unbalanced load. The unbalanced load: $Z_a = 48+12.44\text{i}\ \Omega$, $Z_b = 63+12.44\text{i}\ \Omega$, $Z_c = 98+12.44\text{i}\ \Omega$ [40]. The unbalanced degrees of the output currents in different compensation voltage are illustrated in Fig. 10. The differences in the unbalanced degrees of the output currents among different compensation voltages are manifested in Fig. 11.

It is clearly observed from Fig. 10, the unbalanced degrees of the output currents for the TPTLST and the TPFLST vary with the change of the series-compensating voltage and

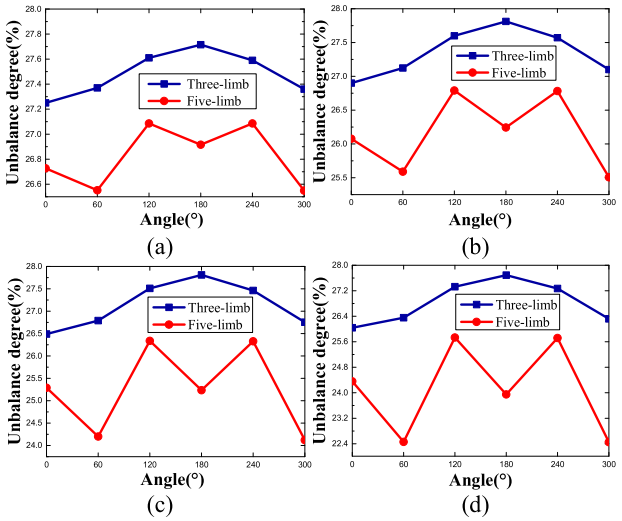

FIGURE 10. Comparison between the unbalanced degrees of the output currents from the TPFLST and the TPTLST (a) ST at $U_{ST} = 0.1$ p.u.. (b) ST at $U_{ST} = 0.2$ p.u.. (c) ST at $U_{ST} = 0.3$ p.u.. (d) ST at $U_{ST} = 0.4$ p.u.

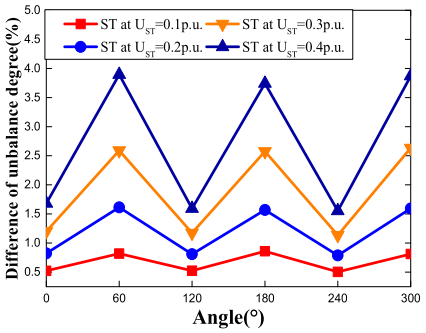

FIGURE 11. The difference of unbalanced degrees of the output current between the TPFLST and the TPTLST.

phase angle under unbalanced load conditions. When β varies between 0° and 360° while U_{ST} keeps to value between 0.1 p.u. to 0.4 p.u. with a step of 0.1 p.u. The range of the unbalanced degrees of output currents for the TPTLST is about from 26.04% to 27.81%. The range of the unbalanced degrees of output currents for the TPFLST is about from 22.45% to 27.09%.

Fig. 11 displays that the differences of unbalanced degrees for the output currents about the TPTLST and the TPFLST increase from 0.504% to 3.895% when the series-compensating voltage rises from 0.1 p.u. to 0.4 p.u. It implies that the unbalanced degrees of the output currents for the TPFLST seem to be better under the working condition of an unbalanced load. Besides, the ST with the five-limb iron-core structure has the end limbs and end yokes comparing with the ST of the three-limb iron-core structure, which provides a low reluctance path for zero-sequence flux. The zero-sequence flux of the three-limb iron-core structure has to complete its path through the tank structure when the ST works under unbalanced load conditions. Nevertheless, the zero-sequence flux of the five-limb iron-core structure can complete its path through the end limbs and the end yokes. As a result, the magnetic flux distribution of the five-limb iron-core structure might be more symmetrical than that for

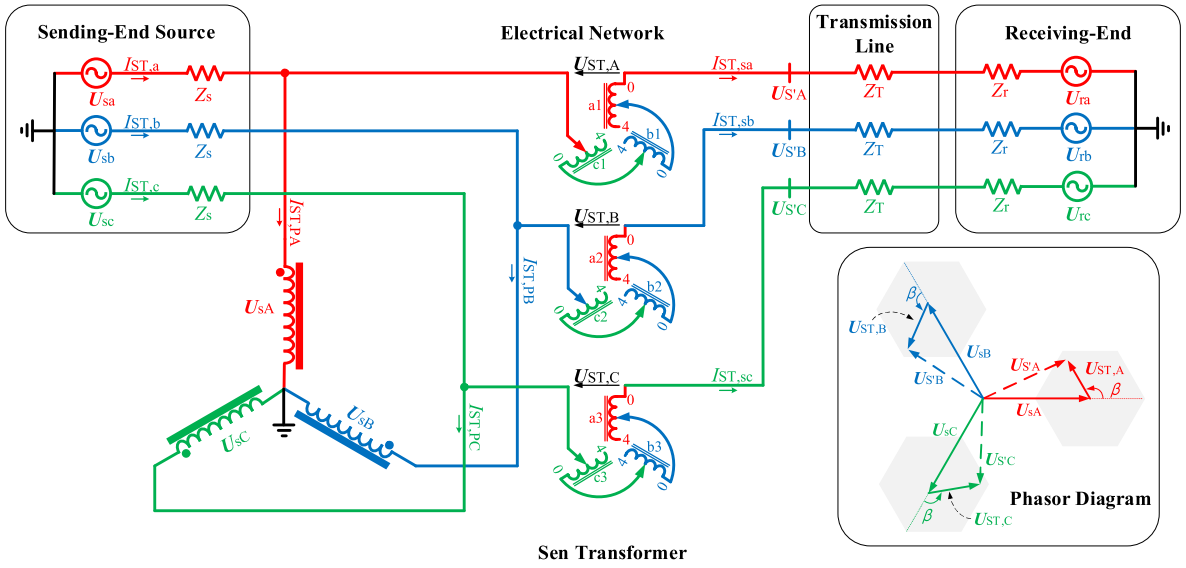

FIGURE 12. The schematic of the ST and its interconnection to the transmission network.

the three-limb iron-core structure, which may decrease the unbalanced degrees of the output currents.

C. DISCUSSIONS

1) PARAMETER DETERMINATION

Some experimental procedures have been reported for the parameter extraction of the kind of duality-based model about the conventional transformer. For instance, Tables 1–3 in [20] showed the test diagrams as well as the equivalent circuits for determining the winding parameters and core parameters of several kinds of conventional transformers. However, it is undeniable that there is no prototype of the three-phase five-limb ST. Therefore, the parameters including the inductances and the resistances describing the iron-core as well as the leakage inductances describing the air-gap have to be estimated by the designed or measured parameters including the geometrical sizes of the similar transformers from the existing literatures. They may be different from the measured parameters for a real ST, which might result in some deviations on the power-flow control performance analysis for the ST.

2) FINITE ELEMENT ANALYSIS

In essence, the accuracy of the duality-based model is relatively limited due to the equivalent process for the electric field and the magnetic field in the transformer. Nevertheless, the finite element method (FEM) can be employed for investigating the detailed behavior of magnetic field, flux density, and core losses, etc., in the transformer. Furthermore, it is important to build a multi-physical field coupling model involving the electric, magnetic, thermal, noising, and vibrating fields for the transformer design [41]. Therefore, a multi-physical field coupling model of ST is essential for analyzing the internal characteristics of ST including the overheat in the windings, the structural stress of iron-core and so on. It is an area worthy of attention.

IV. CONCLUSION

This paper proposes a quasi-steady-state model for the TPFLST using the principle of duality, which takes into consideration of the eddy current effect and the coupling effect involving the magnetic circuit. Two case studies have been carried out on a 138kV and 160MVA TPFLST and its electrical system. There is a good agreement about the series-compensating voltage and the secondary-side current between the results from the proposed model and the ones obtained in the existing literature. Moreover, the unbalanced currents of the STs with different core structures are analysed under unbalanced load conditions. Furthermore, there are some findings as follows.

(1) In the aspect of model applicability, it may efficiently obtain the equivalent circuit model of the TPFLST with the aid of the principle of duality, which can ensure the correctness of its topological structure, and has strong applicability for the STs with different iron-core structures.

(2) In the aspect of electromagnetic coupling, the proposed model considers the phase-to-phase magnetic coupling, the eddy current effect, and the leakage flux between windings, which accurately reflect the internal electromagnetic characteristics of the ST.

(3) In the aspect of iron-core structure, the STs with different iron-core structures have a certain influence on the unbalanced degrees of the output currents. The unbalanced degrees of output currents of the TPFLST are better than that of the TPTLST under unbalanced load conditions, while the differences of unbalanced degrees for the output currents do not exceed 4%.

APPENDIX A
THE ELECTRICAL CONNECTION BETWEEN THE ST AND THE TRANSMISSION NETWORK

See figure 12 here.

APPENDIX B
THE ELEMENTS OF THE ADMITTANCE MATRIX IN (1)

$$
\begin{aligned}
y_{1,1} &= \frac{1}{j\omega L_{a34}} + \frac{1}{\frac{j\omega R_g L_g}{R_g + j\omega L_g} + j\omega L_d} \\
y_{1,2} &= y_{2,1} = -\frac{1}{j\omega L_{a34}}, \\
y_{2,2} &= \frac{1}{j\omega L_{a34}} + \frac{1}{j\omega L_{a23}} \\
y_{2,3} &= y_{3,2} = -\frac{1}{j\omega L_{a23}}, \\
y_{3,3} &= \frac{1}{j\omega L_{a23}} + \frac{1}{j\omega L_{a12}} \\
y_{3,4} &= y_{4,3} = -\frac{1}{j\omega L_{a12}} y_{4,4} = \frac{1}{j\omega L_{a12}} + \frac{1}{\frac{j\omega R_m L_m}{R_m + j\omega L_m} + j\omega L_{a1}} \\
y_{4,5} &= y_{5,4} = -\frac{1}{\frac{j\omega R_m L_m}{R_m + j\omega L_m} + j\omega L_{a1}} \\
y_{5,5} &= \frac{1}{j\omega L_{b34}} + \frac{1}{\frac{j\omega R_y L_y}{R_y + j\omega L_y} + j\omega L_c} + \frac{1}{\frac{j\omega R_m L_m}{R_m + j\omega L_m} + j\omega L_{a1}} \\
y_{5,6} &= y_{6,5} = -\frac{1}{j\omega L_{b34}}, \\
y_{6,6} &= \frac{1}{j\omega L_{b23}} + \frac{1}{j\omega L_{b34}} \\
y_{6,7} &= y_{7,6} = -\frac{1}{j\omega L_{b23}}, \\
y_{7,7} &= \frac{1}{j\omega L_{b23}} + \frac{1}{j\omega L_{b12}} \\
y_{7,8} &= y_{8,7} = -\frac{1}{j\omega L_{b12}}, \\
y_{11,12} &= y_{12,11} = -\frac{1}{j\omega L_{c12}} \\
y_{8,8} &= \frac{1}{j\omega L_{b12}} + \frac{1}{\frac{j\omega R_m L_m}{R_m + j\omega L_m} + j\omega L_{b1}} \\
y_{8,9} &= y_{9,8} = -\frac{1}{\frac{j\omega R_m L_m}{R_m + j\omega L_m} + j\omega L_{b1}} \\
y_{9,9} &= \frac{1}{j\omega L_{c34}} + \frac{1}{\frac{j\omega R_m L_m}{R_m + j\omega L_m} + j\omega L_{b1}} + \frac{1}{\frac{j\omega R_y L_y}{R_y + j\omega L_y} + j\omega L_c} \\
y_{9,10} &= y_{10,9} = -\frac{1}{j\omega L_{c34}}, \\
y_{10,10} &= \frac{1}{j\omega L_{c23}} + \frac{1}{j\omega L_{c34}} \\
y_{10,11} &= y_{11,10} = -\frac{1}{j\omega L_{c23}}, \\
y_{11,11} &= \frac{1}{j\omega L_{c23}} + \frac{1}{j\omega L_{c12}} \\
y_{12,12} &= \frac{1}{j\omega L_{c12}} + \frac{1}{\frac{j\omega R_m L_m}{R_m + j\omega L_m} + j\omega L_{c1}} \\
y_{12,13} &= y_{13,12} = -\frac{1}{\frac{j\omega R_m L_m}{R_m + j\omega L_m} + j\omega L_{c1}} \\
y_{13,13} &= \frac{1}{\frac{j\omega R_m L_m}{R_m + j\omega L_m} + j\omega L_{c1}} + \frac{1}{\frac{j\omega R_g L_g}{R_g + j\omega L_g} + j\omega L_d}
\end{aligned}
$$

APPENDIX C
THE ELEMENTS OF THE DIAGONAL MATRIX K IN (7)

$$
\begin{aligned}
k_1 &= \frac{N_{La1}}{N_H}, \quad k_2 = \frac{N_{Lb1}}{N_H}, \; k_3 = \frac{N_{Lc1}}{N_H}, \\
k_4 &= \frac{N_{La2}}{N_H} \quad k_5 = \frac{N_{Lb2}}{N_H}, \; k_6 = \frac{N_{Lc2}}{N_H}, \\
k_7 &= \frac{N_{La3}}{N_H}, \quad k_8 = \frac{N_{Lb3}}{N_H} \; k_9 = \frac{N_{Lc3}}{N_H}
\end{aligned}
$$

REFERENCES

[1] S. Maihemuti, W. Wang, H. Wang, J. Wu, and X. Zhang, "Dynamic security and stability region under different renewable energy permeability in IENGS system," *IEEE Access*, vol. 9, pp. 19800–19817, 2021.

[2] B. Liu, J. R. Lund, S. Liao, X. Jin, L. Liu, and C. Cheng, "Peak shaving model for coordinated hydro-wind-solar system serving local and multiple receiving power grids via HVDC transmission lines," *IEEE Access*, vol. 8, pp. 60689–60703, 2020.

[3] S. Ganesan, U. Subramaniam, A. A. Ghodke, R. M. Elavarasan, K. Raju, and M. S. Bhaskar, "Investigation on sizing of voltage source for a battery energy storage system in microgrid with renewable energy sources," *IEEE Access*, vol. 8, pp. 188861–188874, 2020.

[4] W. Ma, W. Wang, X. Wu, R. Hu, F. Tang, W. Zhang, X. Han, and L. Ding, "Optimal allocation of hybrid energy storage systems for smoothing photovoltaic power fluctuations considering the active power curtailment of photovoltaic," *IEEE Access*, vol. 7, pp. 74787–74799, 2019.

[5] X. Zhang, Y. Chen, Y. Wang, R. Ding, Y. Zheng, Y. Wang, X. Zha, and X. Cheng, "Reactive voltage partitioning method for the power grid with comprehensive consideration of wind power fluctuation and uncertainty," *IEEE Access*, vol. 8, pp. 124514–124525, 2020.

[6] Q. Wang, Z. Yu, R. Ye, Z. Lin, and Y. Tang, "An ordered curtailment strategy for offshore wind power under extreme weather conditions considering the resilience of the grid," *IEEE Access*, vol. 7, pp. 54824–54833, 2019.

[7] B. Chen, W. Fei, C. Tian, and J. Yuan, "Research on an improved hybrid unified power flow controller," *IEEE Trans. Ind. Appl.*, vol. 54, no. 6, pp. 5649–5660, Nov. 2018.

[8] K. K. Sen and S. M. Ling, "Introducing the family of 'Sen' transformers: A set of power flow controlling transformers," *IEEE Trans. Power Del.*, vol. 18, no. 1, pp. 149–157, Jan. 2003.

[9] A. Kumar and J. Kumar, "Comparison of UPFC and SEN transformer for ATC enhancement in restructured electricity markets," *Int. J. Electr. Power Energy Syst.*, vol. 41, no. 1, pp. 96–104, Oct. 2012.

[10] A. Kumar and C. Sekhar, "Comparison of sen transformer and UPFC for congestion management in hybrid electricity markets," *Int. J. Electr. Power Energy Syst.*, vol. 47, pp. 295–304, May 2013.

[11] K. K. Sen and S. Mey Ling, "Comparison of the 'Sen' transformer with the unified power flow controller," *IEEE Trans. Power Del.*, vol. 18, no. 4, pp. 1523–1533, Oct. 2003.

[12] S. E. G. Mohamed, "Power flow control capability of the power transistor-assisted Sen transformer and the unified power flow controller: A close comparison," *IET Gener., Transmiss. Distrib.*, vol. 14, no. 15, pp. 3033–3041, 2020.

[13] S. E. Gasim Mohamed, J. Jasni, M. A. M. Radzi, and H. Hizam, "Power transistor-assisted sen transformer: A novel approach to power flow control," *Electric Power Syst. Res.*, vol. 133, pp. 228–240, Apr. 2016.

[14] S. E. G. Mohamed, J. Jasni, M. Amran M. Radzi, and H. Hizam, "Implementation of the power transistor-assisted Sen transformer in steady-state load flow analysis," *IET Gener., Transmiss. Distrib.*, vol. 12, no. 18, pp. 4182–4193, 2018.

[15] J. Yuan, L. Liu, W. Fei, L. Chen, B. Chen, and B. Chen, "Hybrid electromagnetic unified power flow controller: A novel flexible and effective approach to control power flow," *IEEE Trans. Power Del.*, vol. 33, no. 5, pp. 2061–2069, Oct. 2018.

[16] H. Song and R. Na, "Out-of-phase technique based few-step type extended 'Sen' transformer and its practical tap selection algorithm," Chinese Patent CN5 262 079 A, Sep. 18, 2017.

[17] T. Behera and D. De, "Enhanced operation of 'Sen' transformer with improved operating point density/area for power flow control," *IET Gener., Transmiss. Distrib.*, vol. 13, no. 14, pp. 3158–3168, 2019.
[18] J. Liu and V. Dinavahi, "Detailed magnetic equivalent circuit based real-time nonlinear power transformer model on FPGA for electromagnetic transient studies," *IEEE Trans. Ind. Electron.*, vol. 63, no. 2, pp. 1191–1202, Feb. 2016.
[19] E. C. Cherry, "The duality between interlinked electric and magnetic circuits and the formation of transformer equivalent circuits," *Proc. Phys. Soc. B*, vol. 62, no. 2, pp. 101–110, 1949.
[20] J. A. Martínez, R. Walling, B. A. Mork, J. Martin-Arnedo, and D. Durbak, "Parameter determination for modeling system transients-Part III: Transformers," *IEEE Trans. Power Del.*, vol. 20, no. 3, pp. 2051–2062, Jul. 2005.
[21] B. A. Mork, "Five-legged wound-core transformer model: Derivation, parameters, implementation and evaluation," *IEEE Trans. Power Del.*, vol. 14, no. 4, pp. 1519–1526, Oct. 1999.
[22] A. Rezaei-Zare, "Enhanced transformer model for low- and mid-frequency transients—Part I: Model development," *IEEE Trans. Power Del.*, vol. 30, no. 1, pp. 307–315, Feb. 2015.
[23] S. Jazebi, S. E. Zirka, M. Lambert, A. Rezaei-Zare, N. Chiesa, Y. Moroz, X. Chen, M. Martinez-Duro, C. M. Arturi, E. P. Dick, A. Narang, R. A. Walling, J. Mahseredjian, J. A. Martinez, and F. de León, "Duality derived transformer models for low-frequency electromagnetic transients—Part I: Topological models," *IEEE Trans. Power Del.*, vol. 31, no. 5, pp. 2410–2419, Oct. 2016.
[24] J. Feng, S. Han, Y. Pan, and X. Hu, "Steady-state modelling of extended sen transformer for unified iterative power flow solution," *Electric Power Syst. Res.*, vol. 187, Oct. 2020, Art. no. 106492.
[25] M. O. Faruque and V. Dinavahi, "A tap-changing algorithm for the implementation of 'Sen' transformer," *IEEE Trans. Power Del.*, vol. 22, no. 3, pp. 1750–1757, Jul. 2007.
[26] Y. Pan, S. Han, C. Zhou, and X. Guo, "On switching transient modeling and analysis of electronic on-load tap-changers based sen transformer," *Int. J. Electr. Power Energy Syst.*, vol. 130, Sep. 2021, Art. no. 107024.
[27] Y. Pan, S. Han, J. Feng, and X. Hu, "An analytical electromagnetic model of 'Sen' transformer with multi-winding coupling," *Int. J. Elect. Power Energy Syst.*, vol. 120, Sep. 2020, Art. no. 106033.
[28] B. Asghari, M. O. Faruque, and V. Dinavahi, "Detailed real-time transient modelof the 'Sen' transformer," *IEEE Trans. Power Del.*, vol. 23, no. 3, pp. 1513–1521, Jul. 2008.
[29] J. Liu and V. Dinavahi, "Nonlinear magnetic equivalent circuit-based real-time sen transformer electromagnetic transient model on FPGA for HIL emulation," *IEEE Trans. Power Del.*, vol. 31, no. 6, pp. 2483–2493, Dec. 2016.
[30] E. Uzunovic, C. A. Canizares, and J. Reeve, "Fundamental frequency model of unified power flow controller," in *Proc. North Amer. Power Symp.*, Cleveland, OH, USA, Oct. 1998, pp. 294–299.
[31] E. Uzunovic, C. A. Canizares, and J. Reeve, "Fundamental frequency model of static synchronous compensator," in *Proc. 29th North Amer. Power Symp. (NAPS)*, Laramie, Wyoming, Oct. 1997, pp. 49–54.
[32] S. V. Kulkarni and S. A. Khaparde, *Transformer Engineering: Design, Technology, and Diagnostics*, vol. 2004, 2nd ed. Boca Raton, FL, USA: CRC Press, 2012.
[33] H. Li, J. Yan, and Y. Liu, "A link-path model-based load-transfer optimization strategy for urban high-voltage distribution power system," *IEEE Access*, vol. 8, pp. 3728–3737, 2020.
[34] C. M. Arturi, "Transient simulation and analysis of a three-phase five-limb step-up transformer following an out-of-phase synchronization," *IEEE Trans. Power Del.*, vol. 6, no. 1, pp. 196–207, Jan. 1991.
[35] S. D. Mitchell and J. S. Welsh, "The influence of complex permeability on the broadband frequency response of a power transformer," *IEEE Trans. Power Del.*, vol. 25, no. 2, pp. 803–813, Apr. 2010.
[36] S. Wang, L. Li, Y. Xie, and G. Zhao, "Electromagnetic characteristic analysis of the series transformer in UPFC system," *Int. J. Appl. Electromagn. Mech.*, vol. 53, no. 3, pp. 469–485, Feb. 2017.
[37] H. Hamzehbahmani, P. Anderson, J. Hall, and D. Fox, "Eddy current loss estimation of edge burr-affected magnetic laminations based on equivalent electrical network—Part I: Fundamental concepts and FEM modeling," *IEEE Trans. Power Del.*, vol. 29, no. 2, pp. 642–650, Apr. 2014.
[38] D. Song, J. Ma, Y. Ma, H. Lin, and S. Liu, "Research on the switching arc loss of on-load tap changer," *IEEE Access*, vol. 7, pp. 180793–180803, 2019.
[39] J. J. Erbrink, E. Gulski, J. J. Smit, P. P. Seitz, B. Quak, R. Leich, and R. Malewski, "Diagnosis of onload tap changer contact degradation by dynamic resistance measurements," *IEEE Trans. Power Del.*, vol. 25, no. 4, pp. 2121–2131, Oct. 2010.
[40] J. Chen, T. Yang, C. O'Loughlin, and T. O'Donnell, "Neutral current minimization control for solid state transformers under unbalanced loads in distribution systems," *IEEE Trans. Ind. Electron.*, vol. 66, no. 10, pp. 8253–8262, Oct. 2019.
[41] C. Liao, J. Ruan, C. Liu, W. Wen, and Z. Du, "3-D coupled electromagnetic-fluid-thermal analysis of oil-immersed triangular wound core transformer," *IEEE Trans. Magn.*, vol. 50, no. 11, pp. 1–4, Nov. 2014.

CHAO ZHOU was born in Guizhou, China, in 1996. He received the B.Sc. degree in electrical engineering from Tianjin University of Technology, Tianjin, China, in 2019. He is currently pursuing the master's degree with Guizhou University. His research interests include power system stability and control, and special transformer research.

SONG HAN (Member, IEEE) received the B.Sc. and M.Sc. degrees from Guizhou University of Technology, Guiyang, China, in 2000 and 2003, respectively, and the Ph.D. degree from Zhejiang University (ZJU), Hangzhou, China, in 2011, all in electrical engineering. He held a postdoctoral position with the Department of Electrical and Computer Engineering, University of Alberta, from 2014 to 2015, and worked as a Western Light Visiting Scholar with ZJU, from 2017 to 2018. He has been a Professor since 2012. He is currently the Director of the Department of Electrical Engineering, Guizhou University. His research interests include AC/DC power system dynamics, FACTS, big data analytics, and its applications in power systems.

NA RONG received the B.Sc. degree in measurement and control technology and instrumentation from Liaoning Technical University, Fuxin, China, in 2001, and the M.Sc. degree in electrical engineering, and the Ph.D. degree in electronic science and technology from Guizhou University, Guiyang, China, in 2009 and 2019, respectively. She is currently a Lecturer with Guizhou University. Her research interests include power system stability and power market.

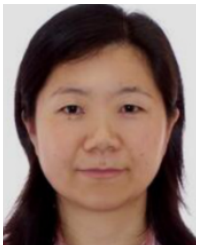

MIN LIU received the Ph.D. degree from The University of Hong Kong. She held a postdoctoral position with The University of Hong Kong, from 2007 to 2008, and a Visiting Scholar with the University of California at Berkeley, Berkeley, from 2013 to 2014. She is currently a Professor and the Vice Dean with the Faculty of Electrical Engineering, Guizhou University, China. Her research interests include smart grid, electricity planning and investment, electricity market, and risk management.